JOURNAL OF SOLID STATE CHEMISTRY 114, 534–538 (1995)

Determination of the Crystallite Size and Shape in Substituted Barium Hexaferrite by X-Ray Line Broadening Analysis

M. V. Cabañas,* P. Germi,† J. M. González-Calbet,‡,§ M. Pernet,† and M. Vallet-Regí*,§,[1]

*Departamento Química Inorgánica y Bioinorgánica, Facultad de Farmacia, Universidad Complutense de Madrid, 28040 Madrid, Spain; †Laboratoire de Crystallographie, CNRS, 166X, 38042 Grenoble, France; ‡Departamento Química Inorgánica, Facultad de Químicas, Universidad Complutense, 28040 Madrid, Spain; and §Instituto de Magnetismo Aplicado, Apdo. 155, Las Rozas, 28230 Madrid, Spain

Received January 13, 1994; in revised form May 31, 1994; accepted June 2, 1994

Platelet-like particles of substituted barium hexaferrite $BaFe_{12-2x}Co_xTi_xO_{19}$ were prepared by the coprecipitation method and the so-called liquid mix technique. The crystallite size (diameter and thickness) has been investigated by X-ray diffraction line-broadening. © 1995 Academic Press, Inc.

INTRODUCTION

The knowledge of the morphology and crystallite size of fine powders is very important in many fields of materials science, such as catalysts and magnetic recording. In this sense, small particles of barium hexaferrite substituted by Co^{2+} and Ti^{4+} ions are suitable for magnetic recording application (1, 2). The size of the platelet-like particles (diameter, thickness) and the diameter/thickness ratio are important factors governing the properties of the barium ferrite medium (3, 4). In this work, the crystallite size of Co–Ti-substituted barium hexaferrite particles has been investigated by X-ray diffraction line-broadening.

EXPERIMENTAL AND DATA ANALYSIS

Samples of $BaFe_{12-2x}Co_xTi_xO_{19}$ ($0 < x < 1$) composition were synthesized by the so-called liquid mix technique and by chemical coprecipitation. Extensive details on the method of synthesis can be found elsewhere (5). In order to study the influence of some synthesis conditions on particle size, two series of the material were prepared by each method.

In the liquid mix technique, chemically pure $Fe(NO_3)_3 \cdot 9H_2O$, $Co(NO_3)_2 \cdot 6H_2O$, $BaCO_3$, $Ti[(CH_3)_2CHO)]_4$, citric acid, and ethylene glycol were used as reagents. After elimination of the organic resin, two material series were obtained which differ in their thermal treatment:

LMT samples: 600°C (70 hr) → 700°C (3 hr) → 800°C (2 hr) → 900°C (1 hr)

LMTR samples: 900°C (1 hr).

In the chemical coprecipitation process, stoichiometric amounts of $Fe(NO_3)_3 \cdot 9H_2O$, $Co(NO_3)_2 \cdot 6H_2O$, $Ba(NO_3)_2$, and $TiCl_4$ were used as raw materials, coprecipitating in a Na_2CO_3/NaOH solution. The coprecipitate obtained was washed with water to pH 7 (CCA samples) or pH 11 (CCB samples). The two material series were subjected to the same accumulative thermal treatment as the LMT samples.

In order to determine the crystal size by the broadening of the Bragg lines, X-ray diffraction patterns of samples synthesized were recorded with a (θ, 2θ) goniometer using Cu$K\alpha$ radiation, operating at 40 kV, 20 mA. The intensities were collected with a step of 0.02° (2θ) and a time of 60 sec per step. Soller slits and a graphite monochromator were interposed in the diffracted beam. Corrections for the instrumental broadening were estimated from the X-ray diffraction data of a bulk $BaFe_{12}O_{19}$ sample prepared by the ceramic method (see Fig. 1). It is worth mentioning that the shape and broadening of the bulk $BaFe_{12}O_{19}$ diffraction lines, have been compared, under the same experimental conditions, to those obtained with well-crystallized materials showing a large crystallite size. The similarity of these lines is evidence that our instrumental profiles do not give great error in our analysis.

The background was removed following the method proposed by Langford (6) which examines the dependency of the variance function ($w(\Delta)$) on the range width of the measures (Δ) for different background values. Then, when $w(\Delta)$ is linear with Δ in an extended angular range, the background has been chosen correctly.

On the other hand, the apparent crystal sizes were deduced from the integral breadth line (β) and by the Fourier method. In the first case, the instrumental correction was performed by the Langford method (7): the recorded line

[1] To whom correspondence should be addressed.

0022-4596/95 $6.00

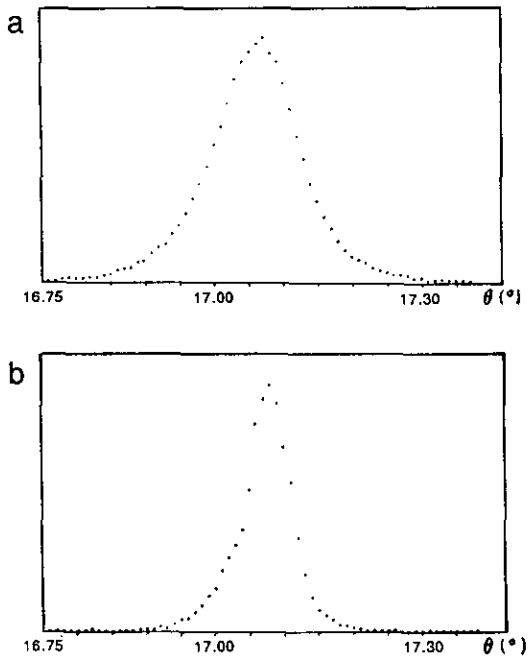

FIG. 1. Diffraction pattern of the (114) Bragg line recorded for (a) a sample obtained by chemical coprecipitation and (b) $BaFe_{12}O_{19}$ reference sample. The broadening of the line is clearly evident.

profiles were fitted to the Voigt function in order to obtain the integral breadth (β). The corresponding apparent sizes (ε_β) were calculated by using the classic Scherrer formula $\varepsilon_\beta = \lambda/\beta \cos \theta$ (8).

In the Fourier analysis, the instrumental correction was carried out by means of the Stokes method (9): $(A_n)_h$ are the samples' Fourier coefficients obtained from the Fourier transform of $I(\theta)$ which were measured in a wide θ range ($\theta_1, \ldots, \theta_2$) around the Bragg angle of the reflection considered. By the same method, the $(A_n)_g$ values corresponding to the instrumental profile's Fourier coefficients were obtained. Then, the Fourier cosine coefficients (A_n), once corrected for the instrumental broadening, were obtained from the $(A_n)_h/(A_n)_g$ ratio. The A_n coefficients are normally expressed as a function of a distance L in the direction normal to the diffracting planes (10) where $L = n\lambda/2(\sin \theta_2 - \sin \theta_1)$, λ being the wavelength and n the Fourier harmonic number. The mean apparent size, ε_F, in a direction perpendicular to the diffracting planes considered, is obtained from the initial slope of the curve of A_n versus L (11) (Fig. 2). However, due to an error in the estimated background level and the fact that the profiles are necessarily truncated at the finite range, a "hook effect" is observed for small values of L in the curve of A_n versus L. This correction was made by means of the procedure suggested by Young *et al.* (12). All the calculations have been made on a Macintosh SE30 microcomputer with programs created by P. Germi.

RESULTS AND DISCUSSION

The chemical analysis performed by inductively coupled plasma shows that initial cationic composition is maintained in all samples. The analysis by flame spectroscopy indicates the presence of 1% sodium in the CCB samples synthesized from the chemical coprecipitation process.

The X-ray diffraction patterns of all synthesized samples show the presence of characteristic reflections of barium hexaferrite (SG $P6_3/mmc$). However, due to the strong overlap of the Bragg diffraction lines, only the (107), (114), (203), and (205) reflections were chosen for the broadening X-ray analysis. According to the procedure explained under Experimental, the apparent crystal sizes obtained from the initial slope of the Fourier transform of the line profile (ε_F), and those corresponding to the integral breadth (ε_β) in the direction perpendicular to the reflecting planes are listed in Table 1. It should be mentioned that the estimated error for both ε_β and ε_F is around ±5%, according to the calculations shown by Langford (13) and Delhez *et al.* (14), respectively. The A_n versus L curves for the four reflections corresponding to the samples synthesized by chemical coprecipitation (samples CCA and CCB for an $x = 0.5$ value) are given in Fig. 2. The results listed in Table 1 show that, in general, the mean size determined by the Fourier method is always smaller than those deduced from the integral breadth, according to the different definitions of both sizes (11, 15). In the same way, the lower apparent size is observed in the direction perpendicular to the (107) diffracting planes, while, in general, the higher value is obtained for the (203) diffracting planes.

In principle, it is difficult to propose some hypotheses about the particle shape from the diffraction data. In addition, the SEM photographs show materials formed by small particles, with no well-defined morphology (Fig. 3).

In general, the crystallite shape is irregular, but in practice the form often approximates, on average, to some regular shape. In this sense, barium hexaferrite particles have a high tendency to crystallize as hexagonal platelets with a high diameter/thickness ratio (16, 17). Then, if we suppose that crystallites can be regarded as cylinders, close to a hexagonal symmetry, with the [001] direction parallel to the cylinder axis (Fig. 4), the angle (φ) between this axis and the diffraction vector [*hkl*]* varies according to [107]* < [205]* < [114]* < [203]* (Table 1). Then, according to the results shown in Table 1, the smaller apparent size corresponding to the direction perpendicular to the (107) planes could be indicative that cylinders must show a high diameter/thickness ratio, so the higher apparent size corresponding to the (203) diffracting planes is associated with a higher cylinder diameter (Fig. 4).

In this sense, if the material belongs to the hexagonal

TABLE 1
Apparent Crystallite Sizes, ε_F and ε_β, Obtained for Different Lines

(a) Samples obtained by the liquid mix technique

		LMT Samples					
		$x = 0.5$		$x = 0.7$		$x = 0.9$	
(*hkl*)	φ (°)	ε_F (Å)	ε_β (Å)	ε_F (Å)	ε_β (Å)	ε_F (Å)	ε_β (Å)
(107)	≃33	319	335	340	377	353	385
(114)	≃63	415	400	431	417	470	454
(203)	≃72	453	457	515	576	549	594
(205)	≃62	400	413	410	436	430	488
		LMTR Samples					
(107)	≃33	310	347	331	348	324	356
(114)	≃63	425	402	452	436	435	421
(203)	≃72	490	502	460	475	497	532
(205)	≃62	400	437	400	428	400	431

(b) Samples obtained by chemical coprecipitation process

		CCA Samples				CCB Samples			
		$x = 0.3$		$x = 0.5$		$x = 0.3$		$x = 0.5$	
(*hkl*)	φ (°)	ε_F (Å)	ε_β (Å)	ε_F (Å)	ε_β (Å)	ε_F (Å)	ε_β (Å)	ε_F (Å)	ε_β (Å)
(107)	≃33	330	384	305	360	360	406	370	428
(114)	≃63	432	474	415	469	550	592	550	600
(203)	≃72	500	511	460	473	660	725	650	700
(205)	≃62	380	412	380	400	500	475	520	517

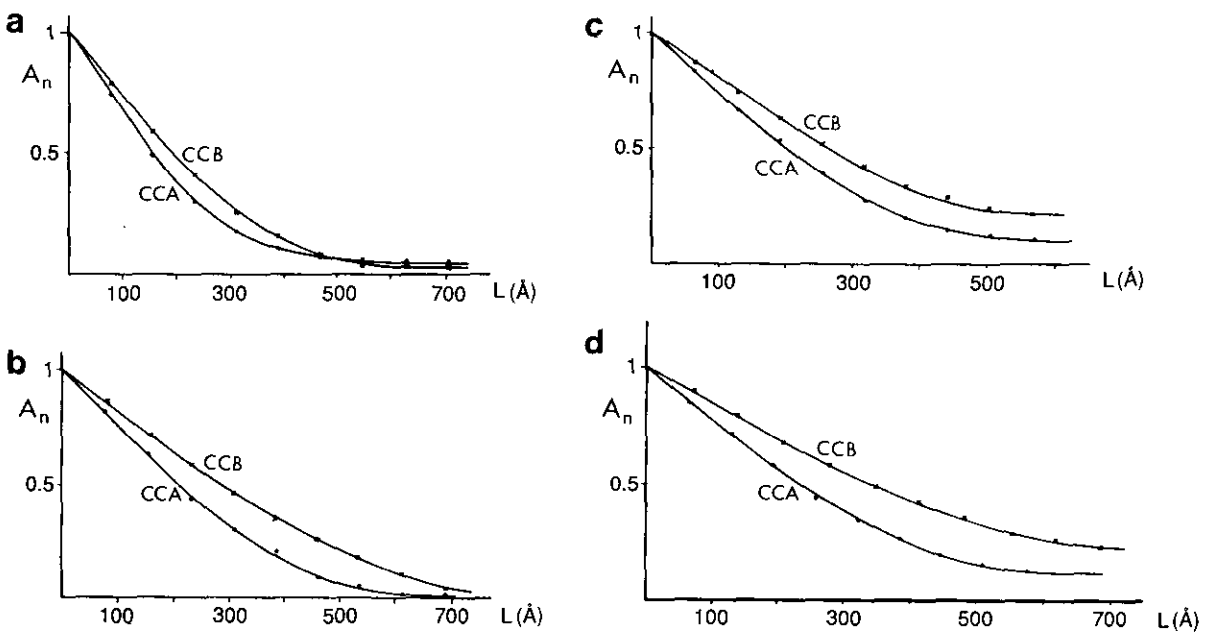

FIG. 2. Fourier cosine coefficients A_n versus L for CCA and CCB samples for (a) (107), (b) (114), (c) (205) and (d) (203) lines.

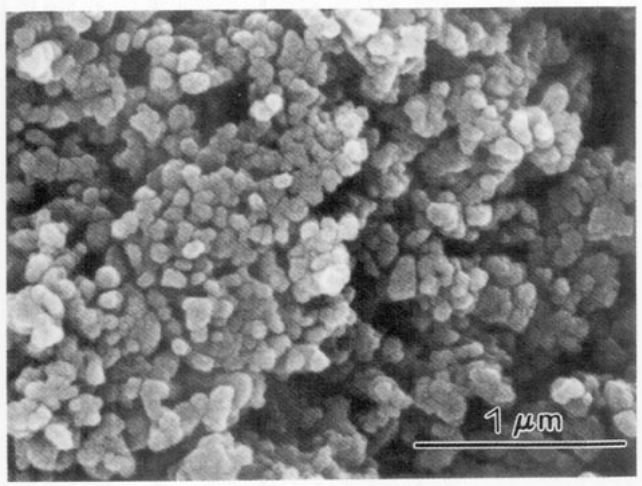

FIG. 3. Scanning electron micrograph of a LMT sample ($x = 0.5$).

TABLE 2
Mean Crystallite Size Obtained from ε_F (*hkl*) Values

Samples	x	D (Å)	H (Å)	D/H
LMT	0.5	1000 ± 50	344 ± 7	2.9 ± 0.1
	0.7	1052 ± 66	367 ± 6	2.9 ± 0.1
	0.9	1180 ± 133	375 ± 12	3.1 ± 0.2
LMTR	0.5	1161 ± 71	319 ± 4	3.6 ± 0.1
	0.7	1050 ± 222	358 ± 19	2.9 ± 0.3
	0.9	1096 ± 107	342 ± 9	3.2 ± 0.2
CCA	0.3	1000 ± 172	361 ± 21	2.8 ± 0.3
	0.5	1054 ± 125	319 ± 8	3.3 ± 0.2
CCB	0.3	2033 ± 292	344 ± 7	5.9 ± 0.2
	0.5	1937 ± 150	357 ± 4	5.4 ± 0.1

Note. D is the diameter, H is the thickness of the platelet and D/H is the diameter/thickness ratio.

system with the c axis parallel to the cylinder axis, the thickness (H) and diameter (D) of the crystallites can be obtained, respectively, from the apparent sizes ε_β following the direction perpendicular to both the (001) and (110) diffracting planes (18). However, this was not possible in our case, due to the overlap of different lines.

On the other hand, the breadth of a small crystallite profile yields an apparent size, ε, which is the weighted average of the dimension of the crystallites in the direction perpendicular to the diffracting planes (19). In order to obtain the cylinder dimensions from the apparent crystal size, it is necessary to know the "true size" (p) generally defined as the cube root of the volume of a crystallite, that is, the product of the apparent size and the appropriate Scherrer constant, K_B ($p = K_B\varepsilon_B$). The value of this constant depends on both the crystallite shape and the breadth line used. In the case of the Fourier method and cylindrical crystals (20),

$$p = \gamma D, \quad \text{where } \gamma = (\pi H/4D)^{1/3} \qquad [1]$$

$$K_F = \gamma[(D/H)\cos\varphi + (H/\pi)\sin\varphi], \qquad [2]$$

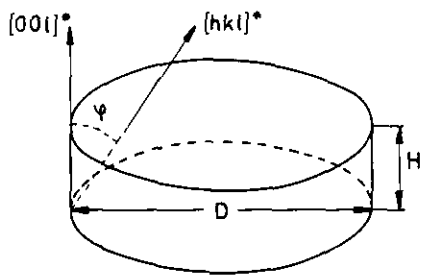

FIG. 4. Platelet-like morphology of the crystallites ($H < D$). D is the mean diameter, H is the thickness, and φ the angle between the cylinder axis and the diffraction vector [*hkl*]*.

where D stands for the cylinder diameter, H for the height, and φ for the angle between the diffraction vector and the cylinder axis (Fig. 4). If we assume that the true size is the same for the different reflections, then

$$K_{F1}\varepsilon_{F1} = K_{F2}\varepsilon_{F2}, \ldots . \simeq \gamma D \qquad [3]$$

$$\frac{K_{F1}}{K_{F2}} = \frac{\varepsilon_{F1}}{\varepsilon_{F2}} = \frac{\cos\varphi_2(D/H) + H\sin\varphi_2}{\cos\varphi_1(D/H) + H\sin\varphi_1}, \qquad [4]$$

thus

$$\frac{D}{H} = \frac{4\pi(\alpha\sin\varphi_2 - \sin\varphi_1)}{\cos\varphi_1 - \alpha\cos\varphi_2} \qquad [5]$$

where $\alpha = \varepsilon_{F2}/\varepsilon_{F1}$.

Then, the D/H ratio and cylinder diameter D can be obtained from the apparent size (ε_F) tabulated in Table 1. The selected reflection pairs were (107) and (114); (107) and (203); (107) and (205), since the vector [107]* is the nearest to the cylinder height and the other vectors are more related to the diameter (Fig. 4). The D and H values obtained applying the above equations are tabulated in Table 2.

It is worth mentioning that although each pair of ε_F values leads to slightly different D and H values, the deviation is small. This can be due to the fact that the above analysis is based on the assumption that all the crystallites have the same size and shape. However, in the actual case there exists a distribution of crystallite sizes and, as a consequence, the definition of the true crystal size is slightly modified (15).

Since the results obtained show a high D/H ratio, the supposition of a platelet shape in our crystals can be accepted. From this model, the crystal dimensions in the

direction of the diffraction vector is, according to Langford and Louer (18),

$$\tau = D/\sin\varphi, \quad \text{for } \varphi \geq \arctan(D/H)$$
$$\tau = H/\cos\varphi, \quad \text{for } \varphi \leq \arctan(D/H)$$

and, $\tau[107]^* < \tau[205]^* < \tau[114]^* < \tau[203]^*$ according to the results obtained (Table 1).

The results in Table 2 show that, for each synthesis method, the mean values of D and H are independent of the Co–Ti content. It is worth mentioning that samples synthesized by the liquid mix technique where Co–Sn was substituted by Fe ions, a progressive enhancement of the mean crystal size with the x value is observed, from 965 Å for $x = 0.2$ to 2245 Å for $x = 0.8$ (20).

In the same way, samples obtained by the same preparation route and with different thermal treatment (samples LMT and LMTR) show equivalent dimensions of greater than 1000 Å for the mean diameter and 300 Å for the thickness. However, in the case of materials synthesized by chemical coprecipitation, the Na presence leads to bigger particles. Thus, in samples CCA, where no sodium was detected, the mean particle size is of the same order as that of samples obtained by the liquid mix technique, with a high D/H ratio. In CCB samples with 1% sodium, the mean particle diameter is clearly higher than that of other samples (~2000 Å), keeping approximately the same thickness when a higher D/H ratio is observed. The different particle size obtained for the samples synthesized by different routes is reflected in their magnetic properties (5).

It may be remarked that, if line broadening is due to the presence of both small crystallite size and microstrain, the treatment becomes more complicated. In this work, the effect of lattice strain has been underestimated. We cannot test for the presence of lattice strain by the experimental method proposed by Williamson and Hall (21) because lines corresponding to multiple orders, for instance, (100) and (200), are not accessible. However, the breadth evolution as a function of θ for comparable directions (for a cylindrical crystal model with the (001) direction parallel to the cylinder axis and $D > H$), such as [114]* and [205]*, shows that if there are microstrains, then they are weak and, as a consequence, could be underestimated. If the microstrains were significant, the breadth of the (205) Bragg line ($2\theta \approx 40°$) should be larger than the (114) one whose Bragg angle is lower ($2\theta \approx 34°$). Since this is not the case (see Table 1), our assumption underestimating the microstrains could be accepted.

The size obtained from the broadening of the Bragg line analysis is of the same order as those obtained from the scanning electron micrographs. This is not necessarily to be expected, as the micrographs give an average agglomerate or grain size, whereas the X-ray technique gives the average size of domains which diffract coherently. Both sizes will be similar only if every grain is a single crystallographic domain. Both techniques are complementary: the scanning electron microscopy gives direct information about the shape and particle size distribution, while the analysis of X-ray diffraction broadening is a method for obtaining the bulk average of the size of coherently diffracting domains. Furthermore, it was possible to calculate the thickness from the broadening of the X-ray diffraction lines. X-ray diffraction gives additional information: each particle observed by scanning electron microscopy is a crystallographic domain, that is, individual particles contain one crystallite.

ACKNOWLEDGMENTS

One of us, MVC, acknowledges the Spanish Ministry of Education for a supporting grant. Financial support from the Comision Interministerial de Ciencia y Tecnología (CICYT, Spain), through Projects MAT91-0331 and MAT93-0207, is also acknowledged.

REFERENCES

1. T. Ido, O. Kubo, and H. Yokoyama, *IEEE Trans. Magn.* **22,** 704 (1986).
2. G. Turilli and A. Paoluzi, *IEEE Trans. Magn.* **24,** 2865 (1988).
3. O. Kubo, T. Ido, H. Yokoyama, and Y. Koike, *J. Appl. Phys.* **57,** 4280 (1985).
4. G. Lisardakis, A. C. Stergiou, J. Georgiu, S. Skabavounos, D. Samaras, M. Pernet, and P. Germi, *J. Magn. Magn. Mater.* **120,** 58 (1993).
5. M. V. Cabañas, J. M. González-Calbet, and M. Vallet-Regí, *J. Solid State Chem.*, (in press).
6. J. I. Langford, *J. Appl. Crystallogr.* **1,** 48 (1968).
7. Th.H. de Keijser, J. I. Langford, E. J. Mittemeijer, and A. B. P. Vogels, *J. Appl. Crystallogr.* **15,** 308 (1982).
8. J. I. Langford, *J. Appl. Crystallogr.* **11,** 10 (1978).
9. A. R. Stokes, *Proc. Phys. Soc. London* **61,** 382 (1948).
10. D. Louer, J. P. Auffredric, J. I. Langford, D. Ciosmak, and J. C. Niepce, *J. Appl. Crystallogr.* **16,** 183 (1983).
11. E. F. Bertaut, *C.R. Seances Acad. Sci.* **228,** 492 (1949); E. F. Bertaut, *Acta Crystallogr.* **3,** 14 (1950).
12. R. A. Young, R. J. Gerdes, and A. J. C. Wilson, *Acta Crystallogr.* **22,** 155 (1967).
13. J. I. Langford, N. B. S. "Special Publication 567. Proceedings, Symposium on Accuracy in Powder Diffraction, NBS, Garthersburg, MD. June 11–15, 1979," pp. 255–269.
14. R. Delhez, Th.H. de Keijser, and E. Mittemeijer, "Special Publication 567. Proceedings, Symposium on Accuracy in Powder Diffraction, NBS, Garthersburg, MD. June 11–15, 1979," pp. 255–269.
15. J. I. Langford and J. C. Wilson, *J. Appl. Crystallogr.* **11,** 102 (1978).
16. M. Kiyama and T. Takada, *Adv. Ceram.* **15,** 61 (1985).
17. M. V. Cabañas, J. M. González-Calbet, M. Labeau, P. Mollard, M. Pernet, and M. Vallet-Regí, *J. Solid State Chem.* **101,** 265 (1992).
18. J. I. Langford and D. Louer, *J. Appl. Crystallogr.* **15,** 20 (1982).
19. A. J. C. Wilson, "X-ray Optics," 2nd ed. Methuen, London, 1962.
20. M. Pernet, X. Obradors, M. Vallet, T. Hernandez, and P. Germi, *IEEE Trans. Magn.* **24,** 1998 (1988).
21. G. K. Williamson and W. H. Hall, *Acta Metall.* **1,** 22 (1953).